

Modeling modern methane emissions from natural wetlands

1. Model description and results

Bernadette P. Walter

Columbia University/NASA Goddard Institute for Space Studies, New York, New York

Martin Heimann

Max-Planck-Institut für Biogeochemie, Jena, Germany

Elaine Matthews

Columbia University/NASA Goddard Institute for Space Studies, New York, New York

Abstract. Methane is an important greenhouse gas which contributes about 22% to the present greenhouse effect. Natural wetlands currently constitute the biggest methane source and were the major source in preindustrial times. Wetland emissions depend highly on the climate, i.e., on soil temperature and water table. To investigate the response of methane emissions from natural wetlands to climate variations, a process-based model that derives methane emissions from natural wetlands as a function of soil temperature, water table, and net primary productivity is used. For its application on the global scale, global data sets for all model parameters are generated. In addition, a simple hydrologic model is developed in order to simulate the position of the water table in wetlands. The hydrologic model is tested against data from different wetland sites, and the sensitivity of the hydrologic model to changes in precipitation is examined. The global methane-hydrology model constitutes a tool to study temporal and spatial variations in methane emissions from natural wetlands. The model is applied using high-frequency atmospheric forcing fields from ECMWF reanalyses of the period from 1982 to 1993. We calculate global annual methane emissions from wetlands to be 260 Tg yr⁻¹. Twenty-five percent of these methane emissions originate from wetlands north of 30°N. Only 60% of the produced methane is emitted, while the rest is reoxidized. A comparison of zonal integrals of simulated global wetland emissions and results obtained by an inverse modeling approach shows good agreement. In a test with data from two wetlands the seasonality of simulated and observed methane emissions agrees well.

1. Introduction

Methane is one of the important greenhouse gases and plays an important role in atmospheric chemistry. Its contribution to the current greenhouse effect is about 22% [Lelieveld *et al.*, 1998]. Ice core records show that the atmospheric methane concentration has varied between 350 ppbv and 700 ppbv during the last 220,000 years until the beginning of industrialization [Jouzel *et al.*, 1993]. Changes in methane concentrations parallel changes in the atmospheric temperature which are inferred from variations in the $\delta^{18}\text{O}$ value. Evidence has been found that at the end of the Younger Dryas, methane increases in Greenland lag the drastic temperature increase by up to a few decades [Severinghaus *et al.*, 1998; Severinghaus and Brook, 1999], suggesting a response of wetland emissions to a climatic change. These climate-induced changes in wetland emissions comprise changes in wetland area and distribution, and changes in methane fluxes, as wetlands are a highly climate-sensitive methane source. Since the beginning of industrialization, the atmospheric methane concentration has increased by a factor of 2.5 and is now 1750 ppbv. In the last two decades

atmospheric methane concentrations have continued to increase and superimposed on this trend is considerable interannual variation [Dlugokencky *et al.*, 1998]. The dramatic increase in the last 200 years has mainly been caused by human activities, though wetlands are believed to contribute considerably to interannual variations and particular anomalies [Hogan and Harris, 1994; Walter *et al.*, this issue].

In this article a global process-based, climate-sensitive model to study climate-induced variations in methane emissions from natural wetlands is presented. The model is based on a one-dimensional model that has been tested thoroughly against high-frequency time series of observations from six different wetlands [Walter *et al.*, 1996; Walter and Heimann, 2000]. The only other global process-based model in the literature was developed by Cao *et al.* [1996]. It calculates present-day global methane emissions from wetlands based on the amount of decomposed organic carbon, water table, and temperature. However, their model has never been tested against time series of methane emission data and has not been applied to temporal variations. In section 2 the methane model and its application on the global scale are described. Section 3 covers global data sets used. The global wetland distribution is prescribed from the data set of Matthews and Fung [1987]. Global data sets of all model parameters, which are soil depth, rooting depth, relative pore space, and efficiency of plant-mediated

Copyright 2001 by the American Geophysical Union.

Paper number 2001JD900165.
0148-0227/01/2001JD900165\$09.00

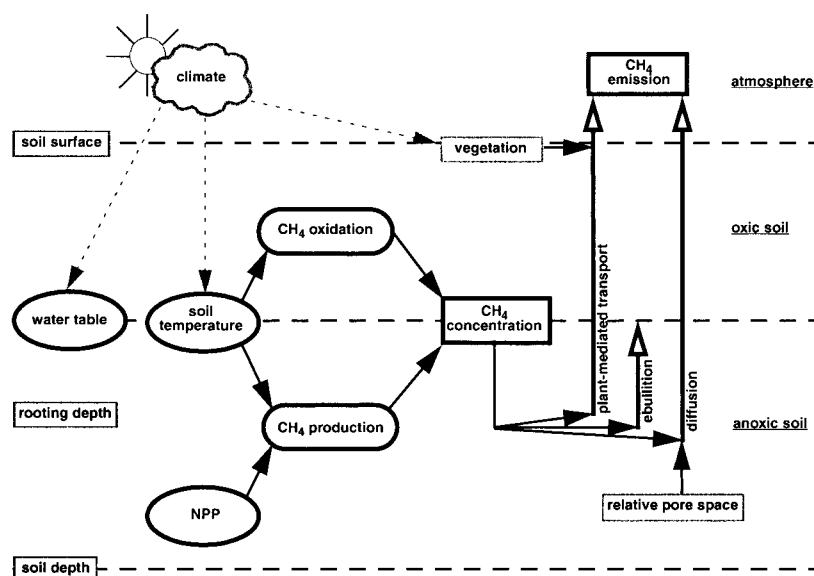


Figure 1. Schematic of the one-dimensional methane model. The processes leading to methane emission to the atmosphere occur in the soil between soil depth and soil surface. Methane production takes place in the anoxic soil below the water table; the methane production rate depends on soil temperature and NPP. Methane oxidation occurs in the oxic soil above the water table and depends on temperature. The model calculates methane concentrations in each (1 cm thick) soil layer. Transport occurs by diffusion through water-/air-filled soil pores, ebullition to the water table, and plant-mediated transport from layers above the rooting depth. Methane emission to the atmosphere is calculated daily.

transport, are developed from existing global data sets of vegetation [Wilson and Henderson-Sellers, 1985] and soil characteristics [Dunne and Wilmott, 1996]. In section 4 the hydrologic model to derive the variation of the water table in wetlands is presented. This includes a model description, tests against observational data, sensitivity tests and global model results of the hydrologic model. In section 5, results of the global methane-hydrology model are shown. They are compared to results obtained by the inverse modeling study of Hein *et al.* [1997] and with field measurements from two wetlands.

2. Methane Model

For global model runs the one-dimensional methane model of Walter and Heimann [2000] is applied to the global wetland distribution of Matthews and Fung [1987]. Figure 1 shows a schematic of the methane model. The model forcing consists of the daily water table, soil temperature, and net primary productivity (NPP). The processes of methane production in the anoxic soil, methane oxidation in the oxic soil, and transport of methane by diffusion, ebullition, and through plants are modeled explicitly in a soil column. The model calculates methane concentration profiles in the soil and methane emissions to the atmosphere on a daily basis [Walter and Heimann, 2000]. Methane production occurs in the anoxic soil between soil depth and water table; production rates depend on substrate availability and soil temperature. Methane oxidation takes place in the oxic soil between water table and soil surface; oxidation rates are controlled by methane concentrations in the soil (using the Michaelis-Menten equation) and soil temperature. Diffusion occurs through the water- or air-filled soil pores and depends on the vertical methane concentration gradient (using Fick's first law) and the relative pore space. Ebullition only takes place in the water-saturated soil where bubbles are formed and

rise to the water table. Plant-mediated transport, which is the transport of methane through the stems of plants, occurs from all soil layers above the rooting depth. It is influenced by the type of vegetation present, which is characterized by the parameter T_{veg} describing the efficiency of plant-mediated transport at a grid cell. Plant-mediated transport varies also as a function of the growing state of plants, which is modeled as a function of soil temperature.

The methane production rate R_{prod} is influenced by soil temperature and NPP, which is taken as a measure of availability of organic carbon for methane production. R_{prod} is parameterized in the following way:

$$R_{prod} = R_0(f(NPP))(f(T_{soil}(t) - T_{mean})). \quad (1)$$

$f(NPP)$ is a function describing the seasonal availability of organic carbon for methane production as well as its distribution with depth. The variation of $f(NPP)$ with time is a function of the relative changes in NPP with time; the vertical distribution of $f(NPP)$ depends on the rooting depth and is constant with time. $f(T_{soil}(t) - T_{mean})$ describes the time evolution of the soil temperature using a Q_{10} dependency ($Q_{10} = 6$; Q_{10} defines the rate of increase in methane production with a 10° temperature increase), whereas $T_{soil}(t)$ is the soil temperature at time t , and T_{mean} is the mean annual soil temperature. R_{prod} is zero at subzero temperatures.

The parameter R_0 is a measure of the amount and quality of substrate for methanogenesis. As the processes determining R_0 are not modeled explicitly, R_0 was adjusted to each of the six data sets used to test the model; the six test sites are located in Michigan, Minnesota, Alaska, Canada, Panama, and Finland. For the global application of the model the value of R_0 for each grid cell, $R_0(x, y)$, is determined using simple multiple linear regression based on the following assumptions. The availability of substrate for methane production is assumed to

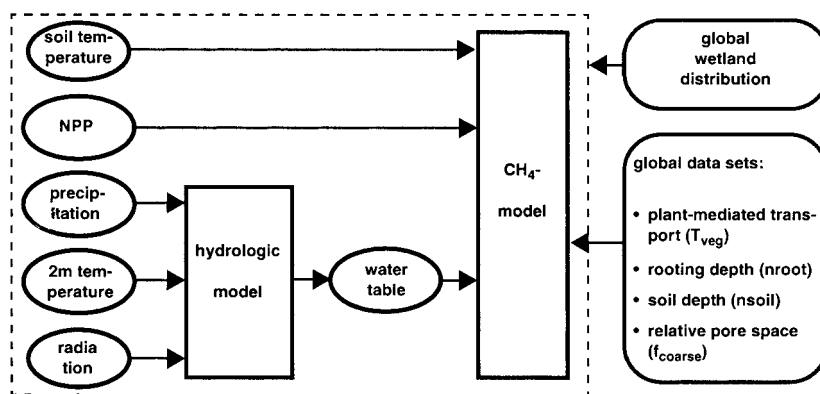


Figure 2. Schematic of the global methane-hydrology model. The forcing of the methane model is soil temperature, NPP, and water table. The water table is calculated from precipitation, 2 m (air) temperature and surface net solar radiation. The global wetland distribution is prescribed using the data set by *Matthews and Fung* [1987]. Global data sets of the model parameters plant-mediated transport, rooting depth, soil depth, and relative pore space are used.

depend on (1) the amount of easily decomposable soil organic matter and (2) the mean annual temperature. (1) The amount of easily decomposable organic matter (from litter production, dead fine roots, and root exudates) is assumed to be connected with NPP. Hence the total annual NPP at a grid cell, $NPP_{tot}(x, y)$, is used as a measure of substrate availability. $NPP_{tot}(x, y)$ is taken from the global terrestrial carbon cycle model Biosphere-Energy Transfer and Hydrology (BETHY) [Knorr, 1997] which calculates NPP for a suite of vegetation types derived from the vegetation map of *Wilson and Henderson-Sellers* [1985]; wetlands are one of the types and are distinguished by an absence of water stress. However, a large fraction of locations identified as wetlands by *Matthews and Fung* [1987] are not primarily wetlands in the vegetation map of *Wilson and Henderson-Sellers* [1985]; wetlands in the vegetation map of *Wilson and Henderson-Sellers* [1985] usually coincide with high fractional inundation in the data set of *Matthews and Fung* [1987] though. Hence in most cases the NPP values from the BETHY model are for nonwetland ecosystems, which constitutes an inconsistency; however, errors are only expected in regions with substantial water stress. (2) The mean annual temperature of the upper 20 cm of soil, $T_{mean}(x, y)$, is taken as a measure of the soil decomposition rate and hence the production rate of substrate for methanogenesis. Using the R_0 values in combination with the respective NPP_{tot} and T_{mean} values from the six test sites of the methane model $R_0(x, y)$ is determined. A simple multiple linear regression yields

$$R_0(x, y) = 0.45 + 0.1 \cdot \frac{T_{mean}(x, y)}{[^{\circ}\text{C}]} - 0.001 \cdot \frac{NPP_{tot}(x, y)}{[\text{gC m}^{-2} \text{yr}^{-1}]}, \quad (2)$$

which shows that $R_0(x, y)$ is mainly dependent upon $T_{mean}(x, y)$. Calculating $R_0(x, y)$ this way considers only substrate quantity. However, substrate quality and the chemical conditions in soil, such as redox potential, pH, and the presence of competing electron acceptors also affect methane production rates, and thus R_0 . A process-based model to predict R_0 from the above mentioned parameters would hence be useful. However, no such model is yet available, partly due to limited knowledge about the quantitative relationships between these parameters and R_0 and because sufficient data on the global distribution of factors affecting R_0 are lacking. However, as

more data become available, a model like that proposed by *Valentine et al.* [1994] and E. A. Holland (unpublished, 2001) could be used to predict R_0 globally.

Figure 2 summarizes model components, forcing data and global data sets used for the global model run; the spatial resolution is 1° by 1° . As mentioned above, the global wetland distribution is taken from the data set of *Matthews and Fung* [1987]. Global data sets of plant-mediated transport (T_{veg}), rooting depth (n_{root}), soil depth (n_{soil}), and relative pore space (f_{coarse}) are derived from existing data sets as described in section 3. A simple hydrologic model is developed to simulate the water table in wetlands, which will be described in section 4. The model forcing consists of soil temperature at several soil depths and NPP (for the methane model), and surface net solar radiation, 2 m (air) temperature, and precipitation (for the hydrologic model).

3. Global Data Sets

3.1. Global Wetland Distribution

The global distribution of natural wetlands is taken from the data set of *Matthews and Fung* [1987] which gives the percentage of wetlands within each 1° by 1° grid cell. However, the data set does not account for seasonal or even interannual variations of wetland areas, and the wetland area given is considered to be the maximum area. The hydrologic model (section 4) simulates the seasonality of the water table at wetland sites and hereby introduces some seasonality. For example, in tropical wetlands, soils dry for a certain period of time; that is, in the model there is no wetland during the dry season (Figure 5, Panama). However, expansion and contraction of wetland areas are not accounted for.

3.2. Global Vegetation Distribution

The global 1° by 1° land cover data set by *Wilson and Henderson-Sellers* [1985] is used to derive all vegetation-dependent parameters. These parameters are the quality of plant-mediated transport (T_{veg}), the rooting depth (n_{root}), and the soil depth (n_{soil}) (Figure 2). *Wilson and Henderson-Sellers* define 53 land cover types, and to each of them relative fractions of 24 possible vegetation types (in the following referred to as WH-vegetation types) are assigned. This means a grid cell

Table 1. Definition of Vegetation Types Used in This Work^a

Types Used in This Work		Types by Wilson and Henderson-Sellers			
Vegetation Type	Description	WH-Vegetation Type	Description		
0	other	1	water		
		2	ice		
		3	inland lake		
		15	arable		
		16	rice		
		17	sugar		
		18	maize		
		19	cotton		
		20	irrigated crop		
		21	urban		
		1	tree	4	evergreen needle leaf tree
5	evergreen broadleaf tree				
6	deciduous needle leaf tree				
7	deciduous broadleaf tree				
8	tropical broadleaf tree				
9	drought deciduous tree				
2	shrub			10	evergreen broadleaf shrub
				11	deciduous shrub
3	short grass			12	thorn shrub
4	long grass	13	short grass and forbs		
		14	long grass		
		22	tundra		
		23	swamp		
		24	soil		

^aAs discussed in section 3.2, the 24 WH-vegetation types of the data set of *Wilson and Henderson-Sellers* [1985] are combined in this work into the following eight vegetation types: tree, shrub, short grass, long grass, tundra, swamp, bare soil, and other. The vegetation type “other” comprises nonnatural “vegetation” types such as urban or arable lands.

can be covered by different fractions of different WH-vegetation types. Combining the 24 WH-vegetation types, as shown in Table 1, reduces the number of vegetation types to the following eight: tree, shrub, short grass, long grass, tundra, swamp, bare soil, and other. The vegetation type “other” comprises nonnatural “vegetation” types such as urban or arable lands. Essentially, the distinction between different types of trees and shrubs is ignored because it is not important for determining the parameters T_{veg} , n_{root} , and n_{soil} .

3.3. Plant-Mediated Transport, T_{veg}

The knowledge about the efficiency of plant-mediated transport by different vegetation types is sparse. Vascular plants can transport gas through their stems. Examples include rice plants [Schütz *et al.*, 1989], *Eriophorum angustifolium* (sedges) [Schimmel, 1995; P. Frenzel, personal communication, 1994] or

Table 2. Parameters T_{veg} , n_{root} , and n_{soil} for Each Vegetation Type

Vegetation Types of This Study	$T_{\text{veg},i}$	$n_{\text{root},i}$, cm	$n_{\text{soil},i}$, cm
0, other	0	0	0
1, tree	1	64	129
2, shrub	0	63	126
3, short grass	10	39	79
4, long grass	15	81	162
5, tundra	10	26	51
6, swamp	15	39	79
7, bare soil	0	0	50

Scheuchzeria palustris (an arrow grass) [Shannon *et al.*, 1996]. While a few plants have been examined for their gas-conducting properties, little is known about the gas-conducting properties of most wetland plants. Therefore several assumptions have been made in this study. It is assumed that plants found growing in wetlands tend to have gas-conducting systems to supply O_2 to their roots, which are often in saturated soil. The vegetation types grasses, tundra, and swamp are considered to have a high potential for plant-mediated transport. Trees, however, do not seem to be good conductors, with the exception of mangroves [Ramachandran and Ramachandran, 1998]. Shrubs are assumed not being capable of transporting gas through their wood stems (P. Frenzel, personal communication, 1998). On the basis of information on vegetation and plant-mediated transport available for the test sites of the methane model [Walter and Heimann, 2000] the unitless parameter T_{veg} , characterizing the efficiency of plant-mediated transport, was defined to range between 0 and 15. T_{veg} of 0 means no plant-mediated transport, 1 poor, and 15 very good plant-mediated transport, respectively. T_{veg} values that were assigned to each vegetation type are summarized in Table 2. The global distribution of $T_{\text{veg}}(x, y)$ is obtained by weighting the T_{veg} values of each vegetation type i , $T_{\text{veg},i}$, with the relative coverage of each vegetation type $p_i(x, y)$ in a grid cell:

$$T_{\text{veg}}(x, y) = \frac{\sum_{i=1}^7 p_i(x, y) T_{\text{veg},i}}{\sum_{i=1}^7 p_i(x, y)}. \quad (3)$$

Only vegetation types 1–7 are considered for natural wetlands since vegetation type 0 does not occur over the distribution of Matthews and Fung’s wetlands. Plate 1a shows the global distribution of the parameter T_{veg} in wetlands.

3.4. Rooting Depth, n_{root}

The rooting depth (n_{root}) is derived from the vertical distribution of the root biomass for different vegetation types given by Jackson *et al.* [1996]. They used an asymptotic, non-linear equation to describe the cumulative root fraction $Y(z)$ at depth z . This equation, taken from a model of vertical root distribution [Gale and Grigal, 1987] is used here:

$$Y(z) = 1 - \beta^z, \quad (4)$$

where β is an extinction coefficient. β values for vegetation types, taken from Jackson *et al.* [1996], were derived from soil studies and biome analyses. The vegetation types used in *Jack-*

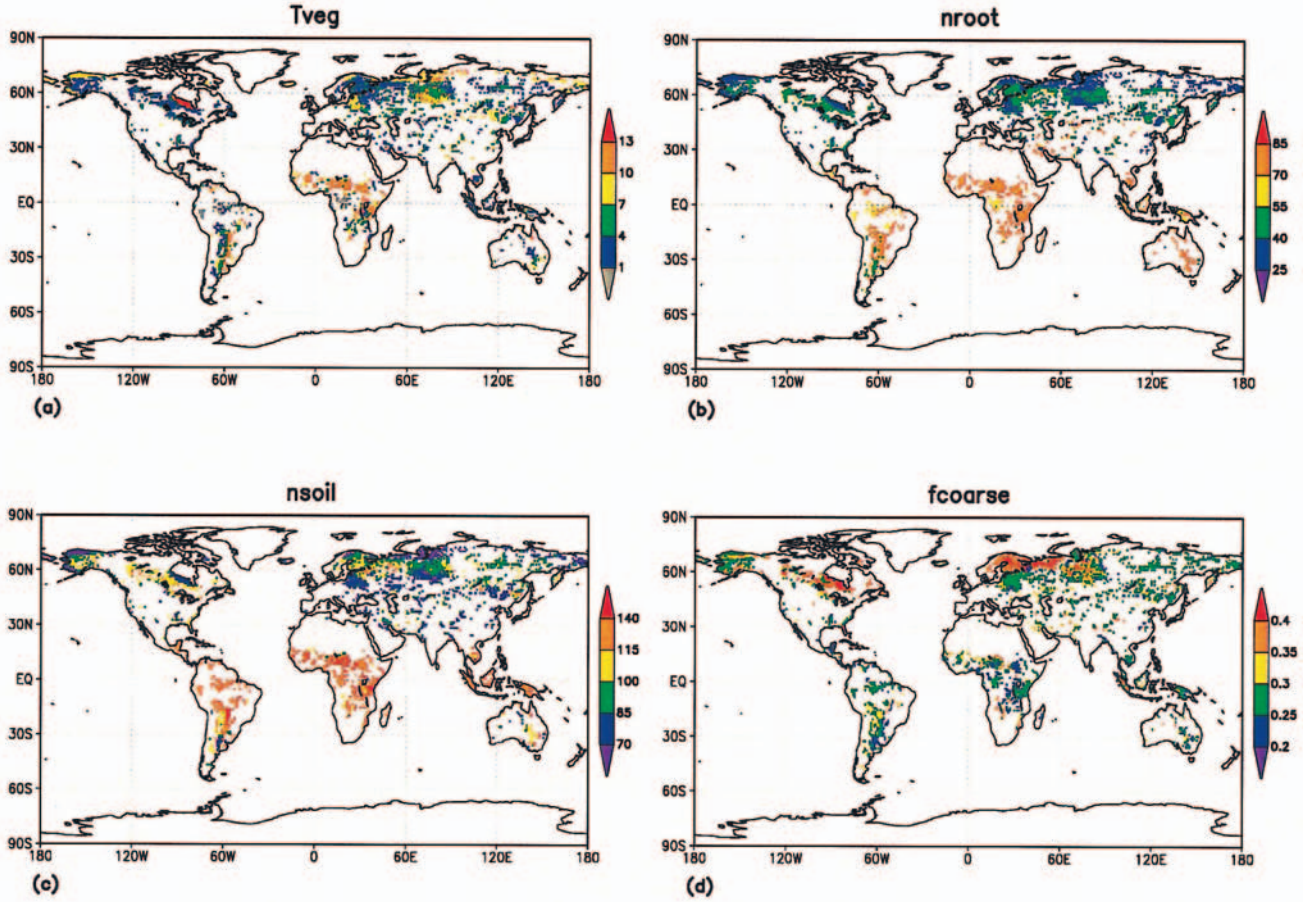


Plate 1. Global distribution of the model parameters: (a) plant-mediated transport, T_{veg} ; (b) rooting depth, $nroot$ (cm); (c) soil depth, $nsoil$ (cm); (d) relative pore space, f_{coarse} .

son *et al.* [1996] are assigned to vegetation types 1–6 used in this article (Table 3). The rooting depths of the vegetation types 0 (other) and 7 (bare soil) are set to 0 cm. From the five β values for forest biomes in the work of Jackson *et al.* [1996], five rooting depths are calculated and averaged to obtain the rooting depth of vegetation type 1 (tree). For vegetation type 6 (swamp) the β value for temperate grassland is used because (1) the biomes of Jackson *et al.* [1996] do not include swamps and (2) the areas denoted as swamps by Wilson and Henderson-Sellers [1985] are located in the same regions as the areas denoted as short grass. The rooting depth $nroot_i$ in centimeters for each vegetation type i is derived by cutting off the cumu-

lative root distribution $Y_i(z)$ in each vegetation type at 90%. Thus $nroot_i$ is obtained by

$$nroot_i = \frac{\ln(1 - Y_i(z))}{\ln \beta} \quad Y_i(z) = 0.9. \quad (5)$$

Table 2 lists the resulting rooting depths. They are similar to rooting depth observations at the test sites of the methane model [Walter and Heimann, 2000]. The rooting depth $nroot_i$ of each vegetation type i is weighted by the relative coverage of each vegetation type $p_i(x, y)$ in a grid cell and by $T_{veg,i}$ because the rooting depth is mainly relevant for plant-mediated transport. Hence the rooting depth $nroot(x, y)$ of a grid cell is calculated from

$$nroot(x, y) = \frac{\sum_{i=1}^6 p_i(x, y) T_{veg,i} nroot_i}{\sum_{i=1}^6 p_i(x, y) T_{veg,i}}. \quad (6)$$

Plate 1b shows the global distribution of rooting depths of wetlands obtained by this method.

3.5. Soil Depth, $nsoil$

The soil depth ($nsoil$) is the lower boundary of the active layer of the methane model, which is that part of soil where

Table 3. Vegetation Types and Extinction Coefficient β

Vegetation Types of This Study	Jackson et al. Vegetation Types	β
1, tree	boreal forest	0.943
	temperate coniferous forest	0.977
	temperate deciduous forest	0.966
	tropical deciduous forest	0.961
	tropical evergreen forest	0.962
2, shrub	sclerophyllous shrubs	0.964
3, short grass	temperate grassland	0.943
4, long grass	tropical grassland	0.972
5, tundra	tundra	0.914
6, swamp	temperate grassland	0.943

methane production occurs. In the methane model, it is assumed that methane is mainly produced from fresh organic material, incorporated in the soil as litter, root exudates, and dead fine roots. Therefore the depth of the active layer (n_{soil}) is linked with the vertical root distribution. Hence n_{soil} is also calculated from the cumulative root fraction $Y(z)$. To obtain n_{soil} , $Y(z)$ is truncated at 99%, because the active layer depth is deeper than the rooting depth due to downward transport of organic matter. The soil depth of vegetation types 0 and 7 is set to 0 and 50 cm, respectively. The resulting values of the soil depth n_{soil} , for each vegetation type i are compiled in Table 2. To obtain the soil depth $n_{\text{soil}}(x, y)$ of a grid cell, the soil depth n_{soil} , is weighted by the relative coverage of each vegetation type $p_i(x, y)$ in the cell. The soil depth $n_{\text{soil}}(x, y)$, in centimeters, is then calculated from

$$n_{\text{soil}}(x, y) = \frac{\sum_{i=1}^7 p_i(x, y) n_{\text{soil}_i}}{\sum_{i=1}^7 p_i(x, y)}. \quad (7)$$

The resulting global distribution of soil depth in wetlands is shown in Plate 1c. Estimates or measurements of the active layer depth lie in the same order of magnitude as the n_{soil} values derived by this method [Walter and Heimann, 2000].

3.6. Relative Pores Space, f_{coarse}

The relative pore space of a soil is determined using the global data set of soil profiles by Dunne and Willmott [1996]. This data set, at a resolution of 0.5° by 0.5° , is based on two soil data sets [M. P. Gildea and B. Moore, 1985; Zabler, 1986], both of which are digital versions of the FAO/UNESCO soil maps [FAO/UNESCO, 1971–1981]. In the data set of Dunne and Willmott [1996], each soil profile is divided in four horizons each with information on soil texture and thickness. Soil texture is expressed in terms of sand, silt, and clay content, and organic soils are also included. In the model the relative pore space is used to calculate diffusion of methane through soil. Therefore the fraction of large, air-filled soil pores is needed. Thus f_{coarse} is determined from the fraction of coarse pores $f_{\text{coarse},j}$ for each horizon j :

$$f_{\text{coarse},j} = (f_{\text{sand},j} p v_{\text{sand}}) + (f_{\text{silt},j} p v_{\text{silt}}) + (f_{\text{clay},j} p v_{\text{clay}}) + (f_{\text{org},j} \cdot p v_{\text{org}}), \quad (8)$$

where $f_{\text{sand},j}$, $f_{\text{silt},j}$, $f_{\text{clay},j}$, and $f_{\text{org},j}$ denote the relative contents of sand, silt, clay, and organic material in each soil horizon j , respectively. $p v_{\text{sand}}$, $p v_{\text{silt}}$, $p v_{\text{clay}}$, and $p v_{\text{org}}$ indicate the relative volume of coarse pores in sandy, silty, clayish, and organic soils, respectively. Based on Hartge and Horn [1991], they are set to 0.45, 0.20, 0.14, and 0.45, respectively. The parameter f_{coarse} is then obtained by averaging the $f_{\text{coarse},j}$ values of all soil horizons. The obtained f_{coarse} values are transformed from a 0.5° by 0.5° grid to a 1° by 1° grid by averaging. The global distribution of f_{coarse} thus obtained is shown in Plate 1d for all wetland grid cells.

4. Hydrologic Model

For this research, a wetland is characterized by a water table at or near the soil surface for a significant part of the year. In

general, inflow and outflow of water are balanced on an annual timescale, although there can be strong seasonal or interannual variations. Input of water includes precipitation, lateral surface or subsurface inflow, and flooding rivers or tides, while outflow can be surface or subsurface outflow and evapotranspiration [Mitsch and Gosselink, 1993]. Climate and topography play a major role; for example, level areas and depressions are favored, and very moist soil conditions lead to slow decomposition rates and hence to the accumulation of organic matter.

The movement of water through soils is affected by gravity and the capillary forces governed by the soil matrix and can be described using two criteria, hydraulic conductivity and water retention characteristics. The hydraulic conductivity depends on the size, form, and continuity of pores in the soil [e.g., Hartge and Horn, 1991] and, in general, is higher in soils with larger pores. Hydraulic conductivity is also a function of the soil water content and increases with increasing soil moisture. Wetlands are characterized not only by high soil moisture but also often by very porous soils, because they generally contain large fractions of organic matter. Therefore they usually have high hydraulic conductivity. The ability of soil to retain water depends mainly on the pore size distribution. In organic soils the pore size distribution is affected by the decomposition stage of the soil. Normally, in a wetland the uppermost layer consists of slightly decomposed peat (fibric peat), the medium layer consists of moderately decomposed peat (hemic peat), and in the deepest layer, the soil is well decomposed (sapric peat) [Letts et al., 2000]. In general, less decomposed soils have larger pores and therefore retain less water. Hence the ability to retain water increases with depth. In this context the water yield coefficient [Boelter, 1968] is a useful parameter since it is a measure of the quantity of water removed from a peat profile when the water table is lowered. It is defined as volume of water, per soil volume, which is removed when the water table is lowered. The water yield coefficient has been found to vary between 0.08 and 0.85 (volume of water/volume of soil) for well-decomposed and undecomposed soils, respectively [Boelter, 1968].

4.1. Model Description

The hydrologic model is built to simulate fluctuations of the water table in wetlands as a function of climate. The position of the water table is calculated on a daily basis using a simple water balance equation. The model forcing comprises daily data on total precipitation and 2 m (air) temperature and 6-hourly data of surface solar net radiation. The spatial resolution is 1° by 1° . It is assumed that hydraulic conductivity is high and that water retention potential increases with depth. Therefore the wetland soil is considered as a simple, modified bucket. This modified bucket, shown schematically in Figure 3, differs from bucket models commonly used for mineral soils and has the following properties: (1) The bucket volume is considered to be the soil pore space between field capacity (originally defined as the amount of water remaining in the soil after the downward movement under gravity has largely ceased [Veihmeyer and Hendrickson, 1931]) and saturation, which means the wetland soil is assumed to be at field capacity at all depths and the hydrologic model calculates where the soil is saturated. (2) It is assumed that the soil is permanently water-saturated below a certain depth which is set to the soil depth n_{soil} . This means that the modified bucket has a lower boundary, n_{soil} , across which no drainage of water occurs. (3) The modified bucket is full below the water table and empty above

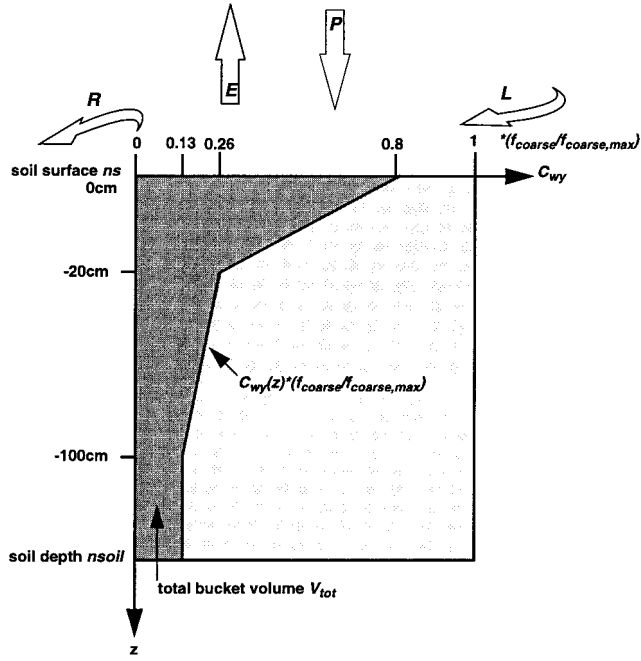


Figure 3. Schematic of the hydrologic model. Input of water occurs by lateral inflow (L) and precipitation (P); outflow of water occurs by evapotranspiration (E) and surface runoff (R). The dark grey area is the total volume of the bucket as defined by equation (10).

it. (4) The modified bucket gets smaller with depth; that is, the water yield coefficient decreases with depth taking into account that the soil is stratified and the water retention potential increases with depth.

The total volume of the bucket (V_{tot}) is calculated using the water yield coefficient (C_{wy}). Based on values reported by *Boelter* [1968], the following values for C_{wy} are chosen: 0.8 at the soil surface, 0.26 at 20 cm depth and 0.13 at 100 cm depth, and C_{wy} is linearly decreasing between those values (Figure 3). V_{tot} is assumed to be larger in soils with a larger relative pore space f_{coarse} . Hence the function $f_{wy}(z)$ describing the amount of water removed from depth z when the water table is lowered below depth z is defined by

$$f_{wy}(z) = C_{wy}(z) \frac{f_{\text{coarse}}}{f_{\text{coarse,max}}}, \quad (9)$$

where f_{coarse} is the relative volume of coarse pores at a grid cell, and $f_{\text{coarse,max}}$ is the maximum global value of f_{coarse} . $C_{wy}(z)$ denotes the variation of C_{wy} as a function of depth z . Using $f_{wy}(z)$, V_{tot} is calculated by integrating over the whole soil depth

$$V_{\text{tot}} = \int_{n\text{soil}}^{ns} f_{wy}(z) dz, \quad (10)$$

where $n\text{soil}$ is the lower boundary of the bucket, and ns is the soil surface. The unit of V_{tot} is in centimeters (multiply by respective wetland area to get a volume). The hydrologic model is initialized with a full bucket and run to equilibrium, so results are independent of initial conditions.

The following ways of inflow and outflow of water are considered. Input of water can be precipitation and lateral inflow,

and removal of water occurs by evapotranspiration and runoff. There is currently no distinction between lateral surface and subsurface flow. Since wetlands usually form under conditions where lateral outflow is inhibited (e.g., by topography), only surface runoff is considered. Lateral inflow is taken into account only in arid regions. The volume of water stored in the bucket (V_{wat}) is calculated daily, and day-to-day changes in V_{wat} are calculated solving the water balance equation

$$\frac{d}{dt} V_{\text{wat}}(t) = P(t) - ET(t) + L(t) - R(t), \quad (11)$$

where $P(t)$ denotes precipitation, $ET(t)$ evapotranspiration, $L(t)$ lateral inflow of water, and $R(t)$ surface runoff. $P(t)$, $ET(t)$, $L(t)$, and $R(t)$ are given in cm d^{-1} , while the unit of $V_{\text{wat}}(t)$ is in centimeters.

4.1.1. Evapotranspiration. Evapotranspiration includes evaporation from the soil surface and transpiration by plants. The actual evapotranspiration (ET) rate is limited by the supply of water from the soil. Hence $ET(t)$ is calculated from

$$ET(t) = \min(\text{demand}(t), \text{supply}(t)). \quad (12)$$

$\text{Supply}(t)$ denotes the actual evapotranspiration rate restricted by availability of water in the soil. $\text{Demand}(t)$ is calculated using the equilibrium evapotranspiration rate derived from the energy balance between net radiation, latent and sensible heat fluxes, and ground heat flux at the soil surface. Assuming that the ground heat flux is small compared to the latent and sensible heat fluxes, $\text{demand}(t)$ is calculated after *Slatyer and McIlroy* [1961]:

$$\text{demand}(t) = [s_T(t)/(s_T(t) + \gamma)](\text{rad}(t)/\lambda), \quad (13)$$

where λ is the latent heat of evaporation (2.45 MJ kg^{-1} at 20°C), and γ is the psychrometric constant of about 65 Pa K^{-1} . $\text{Rad}(t)$ denotes the net radiation at the soil surface calculated as the sum of the surface solar and thermal radiation; $s_T(t)$ denotes the temperature derivative of the saturation vapor pressure curve, de_s/dT , whereby the saturation vapor pressure e_s is calculated after the *Mangus* formula [e.g., *Murray*, 1967]. Hence $s_T(t)$ yields

$$s_T(t) = \lambda \frac{e^{[l_1 - T_{2m}(t)]/l_2 + T_{2m}(t)}}{l_2 + T_{2m}(t)^2}, \quad (14)$$

where $T_{2m}(t)$ is the air temperature at 2 m height, and l_1 and l_2 are constants, which are 17.269 and 237.3, respectively. If the soil does not contain enough water to evaporate at the equilibrium evapotranspiration rate, the actual evapotranspiration rate is calculated after *Federer* [1982]:

$$\text{supply}(t) = c \frac{V_{\text{wat}}(t)}{V_{\text{tot}}}, \quad (15)$$

where V_{tot} is the maximum bucket size, and $V_{\text{wat}}(t)$ is the volume of water stored in the bucket at time t . c is a factor (cm d^{-1}) which depends on $V_{\text{wat}}(t)$ and the relative vegetation coverage of the soil,

$$c = \begin{cases} 1.5 & \text{if } (V_{\text{wat}}(t) \geq V_{\text{tot}}) \\ 0.24 + 0.96 \cdot \frac{100 - p_{\text{bare}}}{100} & \text{else} \end{cases}, \quad (16)$$

where p_{bare} denotes the percentage of unvegetated, bare soil, which is derived from the global land cover data set by *Wilson and Henderson-Sellers* [1985]. Maximum supply rates of 1.5 cm d^{-1}

d^{-1} are used for grid cells with standing water (i.e., if $V_{\text{wat}}(t) \geq V_{\text{tot}}$), while 0.24 and 1.2 cm d^{-1} are used for unvegetated and for totally vegetated grid cells, respectively, according to Kaduk [1996].

4.1.2. Lateral inflow. Some wetlands occur in arid regions where wetlands would not be located if precipitation were the only source of water. In the hydrologic model, a region is defined to be arid, if the difference between total annual precipitation and total annual potential evapotranspiration (PmE) is negative. These wetlands are most likely fed by lateral inflow of water from higher lands, lakes, and/or rivers; the Niger and the Parana are examples of these arid wetlands. To maintain wetland conditions, the annual inflow of water to a wetland must be equal or greater than the annual outflow. Therefore the lateral inflow $L(t)$ is introduced to close the water balance in regions where PmE is negative. For the sake of simplicity, potential sources of lateral inflow, such as higher lands, rivers, or lakes, are not distinguished. The different origins of lateral inflow would affect its seasonality. Instead, the amount of water needed to close the annual PmE balance is added to the bucket at a constant daily rate throughout the year. Hence $L(t)$ is calculated from

$$L(t) = \begin{cases} 0 & \text{if (PmE} > 0) \\ \frac{-\text{PmE}}{\text{days}} & \text{else} \end{cases}, \quad (17)$$

where days denote the number of days of the year. The parameterization of $L(t)$ constitutes a strong simplification. However, since only wetlands are considered, $L(t)$, if not zero, is small compared to the other components of (11). In reality, there is also lateral inflow of water in nonarid regions. In the hydrologic model, however, this is compensated for by higher runoff, since the model is run in equilibrium on an annual basis. Therefore ignoring lateral inflow in nonarid regions does not affect simulated water table levels very much.

4.1.3. Runoff. It is assumed that wetlands are typically located in regions where lateral drainage is inhibited. Therefore only surface runoff, $R(t)$, is considered. In the hydrologic model, runoff occurs only in conditions of standing water, i.e., if $V_{\text{wat}}(t) > V_{\text{tot}}$. The amount of outflow via runoff is assumed to depend on the height of the standing water and the terrain steepness. It is calculated from

$$R(t) = \begin{cases} 0 & \text{if } (V_{\text{wat}}(t) < V_{\text{tot}}) \\ H_{\text{wt}}(t) \left\{ \frac{H_{\text{wt}}(t)^2}{k_1} + \frac{S}{k_2} \right\} & \text{else} \end{cases}. \quad (18)$$

S is the Laplace operator of the terrain height (i.e. $S = |\Delta \text{terrain height}|$), which is derived from the 5' by 5' topographical data set ETOPO5 [Edwards, 1989] and interpolated to the 1° by 1° resolution. $H_{\text{wt}}(t)$ is the height of the water table relative to the soil surface in centimeters, and k_1 and k_2 are constants, which are set to 1500 d cm^2 and 2000 d, respectively; k_1 and k_2 are chosen in such that (1) ~50–90% of the standing water is removed daily by runoff and (2) influences of $H_{\text{wt}}(t)$ and the terrain slope S on runoff are balanced in situations with average values for S and $H_{\text{wt}}(t)$ (~10 cm). Sensitivity tests have shown that the results of the hydrologic model are not very sensitive to the choice of k_1 and k_2 [Walter, 1998].

4.2. Results and Discussion

4.2.1. Tests against observational data. The hydrologic model simulates the position of the water table in the wetland fraction of a 1° by 1° grid cell. A single “mean” water table level is calculated for the wetland fraction of cells, thereby neglecting that soils are heterogeneous and the position of the water table usually varies within a wetland due to microtopography. The possible effects of neglecting microtopography on simulated methane emissions is tested and discussed by Walter *et al.* [this issue]. For the test against water table observed at field sites, the required inputs for the hydrologic model (precipitation, surface solar net radiation, and 2 m temperature) were not available. Therefore the European Centre for Medium-Range Weather Forecasts (ECMWF) reanalyses [Gibson *et al.*, 1997] were used as forcing (section 5.1). Since the variability of the input data, particularly precipitation, within one grid cell is usually quite high, the ECMWF input data probably differ from the actual input data at the respective sites. Hence a more rigorous test of the hydrologic model would include field input data. However, in a test using reanalyses the ability to reproduce seasonal patterns and the magnitude of observed water table fluctuations can be examined.

Water table data are available from the test sites of the methane model [Walter and Heimann, 2000]. Observed water table levels are compared to simulated water table levels of the grid cell where the test site is located. Figure 4 shows the results at four sites located in Finland and the United States (Alaska, Minnesota, and Michigan). The observations are from Saarnio *et al.* [1997] (Finland), Whalen and Reeburgh [1992] (Alaska), Dise [1993] (Minnesota), and Shannon and White [1994] (Michigan). At most sites, measurements at several different microsites within the wetland were performed. The data show that within one site, water table levels can differ by several tens of centimeters between hummock and hollow structures, for example, at the sites in Finland and Minnesota. The seasonal patterns and magnitudes of water table fluctuations are reproduced reasonably by the hydrologic model at most sites. However, at the Minnesota and Michigan sites the amplitude of simulated water table levels is overestimated. This could be due to the form of the function $C_{\text{wy}}(z)$, which decreases strongly from the soil surface to 20 cm soil depth and is small below -20 cm. Hence below 20 cm soil depth, the removal of a fixed amount of water translates into a much bigger decline in water table than in the upper 20 cm of soil. This could explain the sharp decrease in simulated water table levels in Figures 4c and 4d. The global model runs combining the hydrologic and methane models were performed using this version of the hydrologic model. In the future, different formulations of $C_{\text{wy}}(z)$ should be tested in order to further improve the hydrologic model. Figure 8 shows another comparison of simulated water tables with observations.

4.2.2. Sensitivity tests. The sensitivity of the hydrologic model to changes in the parameters k_1 and k_2 (equation (18)) and in precipitation was evaluated. Model results are not very sensitive to k_1 and k_2 , whether or not standing water occurs rarely or often, nor how high the water table is above the soil surface [Walter, 1998]. The results of the sensitivity test to changes in precipitation are shown in Figure 5 for six grid cells from different regions representing a variety of soil and climatic conditions. The model was forced with ECMWF reanalyses for 1988. Three runs were performed using 100% precipitation (control), 80% precipitation, and 120% precipitation.

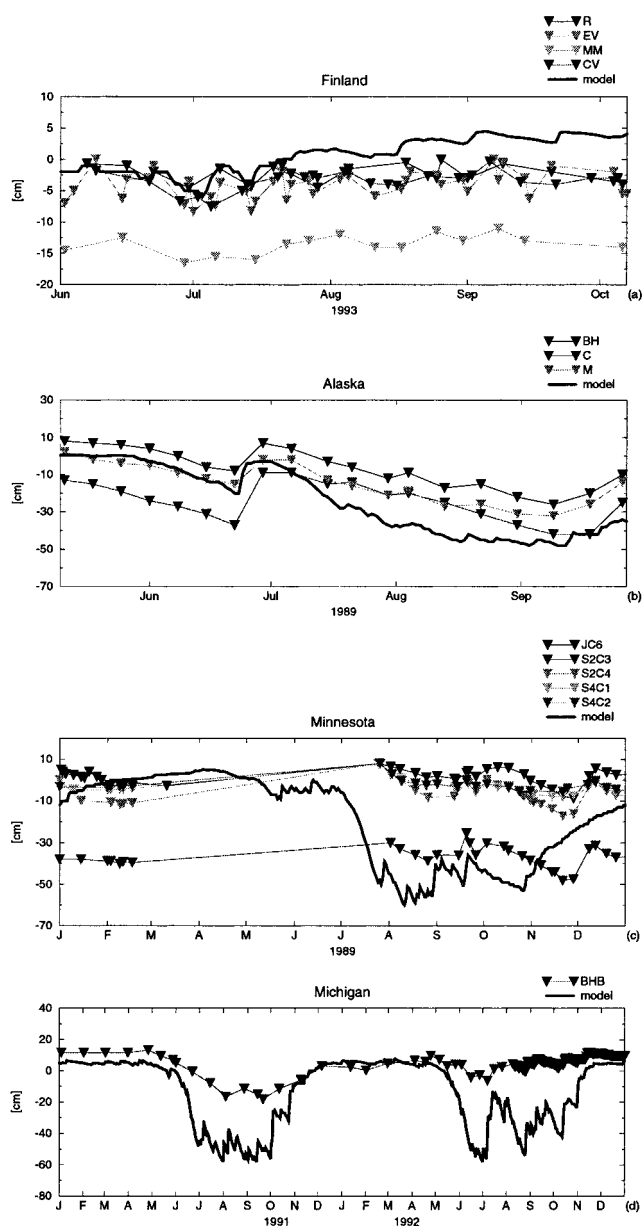


Figure 4. Results of tests of the hydrologic model against data from four wetlands (different sets of triangles indicate different sites within the same wetland). Modeled water tables (in centimeters) (thick lines) and observed water tables (triangles) from (a) Finland (Saarnio *et al.* [1997]), (b) Alaska (Whalen and Reeburgh [1992]), (c) Minnesota (Dise [1993]), and (d) Michigan (Shannon and White [1994]). Note that y-axis units differ.

Greater precipitation generally leads to higher water table levels and vice versa, but the relative effect of a 20% increase or decrease in precipitation varies among sites. For example, the effect is large at the Alaskan and the Finish sites but small at the Minnesotan or Michigan sites. In general, a $\pm 20\%$ change in precipitation has a smaller effect at sites where precipitation is higher, and vice versa [Walter, 1998]. Therefore the effect is smaller at most tropical sites as, for example, in Panama (see also Plates 2e, 2f). In the tropics, precipitation is extremely low during the dry season and a $\pm 20\%$ change does not change much; during the wet season, precipitation is very

high causing standing water, and a $\pm 20\%$ change only changes the amount of runoff. However, in some tropical regions, greater precipitation can cause lower water table levels, and vice versa (Chad). This occurs in arid regions, where PmE is negative and the lateral inflow, L , (equation (17)) is different from zero. L is calculated every year and is smaller in years with greater precipitation, and vice versa. Different L values due to different precipitation affect the water table mainly during the dry season. Since most methane emissions take place in the wet season, it is not expected to change modeled methane emissions very much (see also Walter *et al.* [this issue]). However, this problem will be fixed in future versions of the model.

The results of the same sensitivity test ($\pm 20\%$ precipitation) are plotted globally as annual means in Plates 2e, 2f. At most places, reduced precipitation leads to lower annual water table levels, and vice versa. The arid regions, where owing to the parameterization of the lateral inflow, L , the opposite happens, are some regions in Africa and South America. Considering only those places where changes in precipitation and water table have the same sign, Plate 2 shows that $\pm 20\%$ changes in precipitation have a stronger effect in the HNH than in the tropics, as explained in the last paragraph.

4.2.3. Water table in wetlands and its seasonality. Plates 2a–2d show global results of the hydrologic model for wetland points only. Monthly mean water table levels are plotted for February, May, August, and November. In high Northern Hemisphere ($>30^\circ\text{N}$, HNH) wetlands the water table is high during the winter and low during the summer. In tropical wetlands the water table is low during the dry season, which lasts from February to May in Northern Hemisphere tropics and from August to November in Southern Hemisphere tropics. The amplitudes of variations in the water table are generally larger in the tropics with standing water during the wet season and water levels below 1 m soil depth (Figure 5, Panama) during the dry season.

4.2.4. Hydrologic model: limitations. Although the hydrologic model is a relatively simple approach, the results of the comparison between modeled and observed water table levels illustrate that it yields realistic results. As discussed in section 4.2.1, different choices of the function $C_{wy}(z)$ should be tested, and the parameterization of the lateral inflow, L , should be improved in the future. In addition, the following three factors not yet considered may be important: (1) the contribution of permafrost, (2) snow, and (3) wetland microtopography. (1) In permafrost soils, water is stored in the form of ice until the soils thaw. Furthermore, surface water cannot infiltrate into a frozen soil. Both facts favor saturation of surface soils in spring. While the hydrologic model performs well at the Alaskan site, which is underlain by permafrost, further tests with data from other permafrost sites should be conducted. (2) Water is also stored in the form of snow until the snow melts. This also favors saturation of surface soils in spring. However, the model results do not differ systematically from observations in spring. (3) The position of the water table calculated by the hydrologic model can be viewed as a “mean” water table level of a wetland. However, complex microtopography can result in water table levels that vary by several tens of centimeters on small spatial scales (i.e., in the order of meters). The methane model is quite sensitive to the position of the water table mostly due to efficient oxidation of methane in oxic surface soils. Therefore neglecting the effects of microtopography on the water table can affect modeled methane

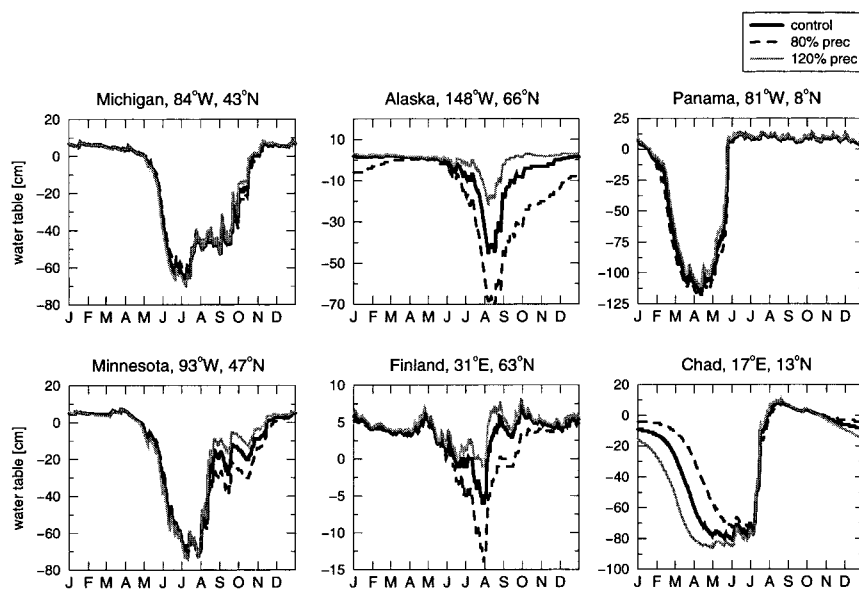


Figure 5. Sensitivity test of the hydrologic model to precipitation. Simulated water table (in centimeters) for the control run with 100% precipitation (black), the run with 80% precipitation (dashed), and the run with 120% precipitation (grey). Note that y-axis units differ.

emissions as discussed by *Walter et al.* [this issue]. Hence micropography should be included into a future version of the hydrologic model.

5. Results of the Global Methane-Hydrology Model

5.1. Model Forcing

The forcing for the global methane-hydrology model is shown in Figure 2. This paper reports on model runs using the European Centre for Medium-Range Weather Forecast (EC-MWF) reanalyses [*Gibson et al.*, 1997] for the period 1982–1993 for the climate forcing. The forcing data are in T106 resolution (T106-truncation corresponds to 1.1° by 1.1°) and are linearly interpolated to a 1° by 1° grid. We use 24-hourly forecasts of total precipitation and soil temperature at several soil depths (4, 18, 64, and 195 cm below the soil surface, linearly interpolated to 1 cm intervals) and 6-hourly forecasts of the 2 m (air) temperature, and surface solar and thermal radiation. 6-hourly forecasts are available 4 times a day and are used in cases where a diurnal cycle is needed. For precipitation, 24-hourly forecasts are used because they yield better precipitation results than forecasts over shorter periods [*Stendel and Arpe*, 1997]. Daily net primary productivity (NPP) is obtained from monthly NPP values calculated by the global terrestrial carbon cycle model Biosphere-Energy Transfer and Hydrology (BETHY) [*Knorr*, 1997]. The BETHY model is a process-based model describing the water balance on vegetated surfaces and bare soils and the CO₂ balance in vegetation and soils. It uses remote sensing data and calculates the NPP on a 0.5° by 0.5° grid with monthly time steps. The output of the BETHY model is linearly interpolated to daily values on a 1° by 1° grid.

5.2. Global Methane Emissions From Wetlands

Plate 3a shows the average of the simulated mean annual methane fluxes from natural wetlands for 1982–1993. Mean

annual fluxes range from a few mg m⁻² d⁻¹ to more than 400 mg m⁻² d⁻¹. Per grid cell methane emissions in Gg yr⁻¹ calculated using the actual wetland areas of each wetland grid cell are plotted in Plate 3b. Simulated mean annual fluxes are usually larger in lower latitudes where growing season lengths are longer; also, they are usually larger in regions where annual total fractional oxidation (the percentage of produced methane that is reoxidized before reaching the atmosphere (Plate 3c)) is lower. In the only other global modeling study of methane emissions from wetlands, *Cao et al.* [1996] find a similar spatial pattern of annual methane emissions from wetlands; however, their global wetland source strength is 92 Tg yr⁻¹ and hence considerably lower than in this study (section 5.2.1). In the model, globally and annually, only about 60% of the produced methane is emitted; the rest is reoxidized in soil. Annual total fractional oxidation is the sum of annual soil oxidation (Plate 3d) and annual rhizospheric oxidation (Plate 3e). The data in Plate 3b are used to convert fractional oxidation (%) into amounts of methane emitted. As discussed by *Bogner et al.* [2000], in the methane model, soil oxidation is controlled by the position of the water table, and rhizospheric oxidation by vegetation. If the water table is below the soil surface, methane is partly oxidized in the oxic top soil. In northern high-latitude wetlands, for example, annual soil oxidation is larger in regions where the water table is lower during the active season (compare Plates 2a–2d and Plate 3d). Part of the methane entering plants is oxidized in the rhizosphere (sections 2 and 3.3), increasing rhizospheric oxidation and hence total fractional oxidation. If the water table is below the soil surface, however, methane transported through plants bypasses the oxic top soil, leading to decreased soil oxidation and hence reduced total fractional oxidation. Therefore regions where rhizospheric oxidation is large can still be regions where methane fluxes are large, since the fraction of methane emitted through plants is also large.

Zonally integrated annual methane emissions over the period 1982–1993 are shown in Figure 6a. The comparison with the results of an inverse modeling study by *Hein et al.* [1997]

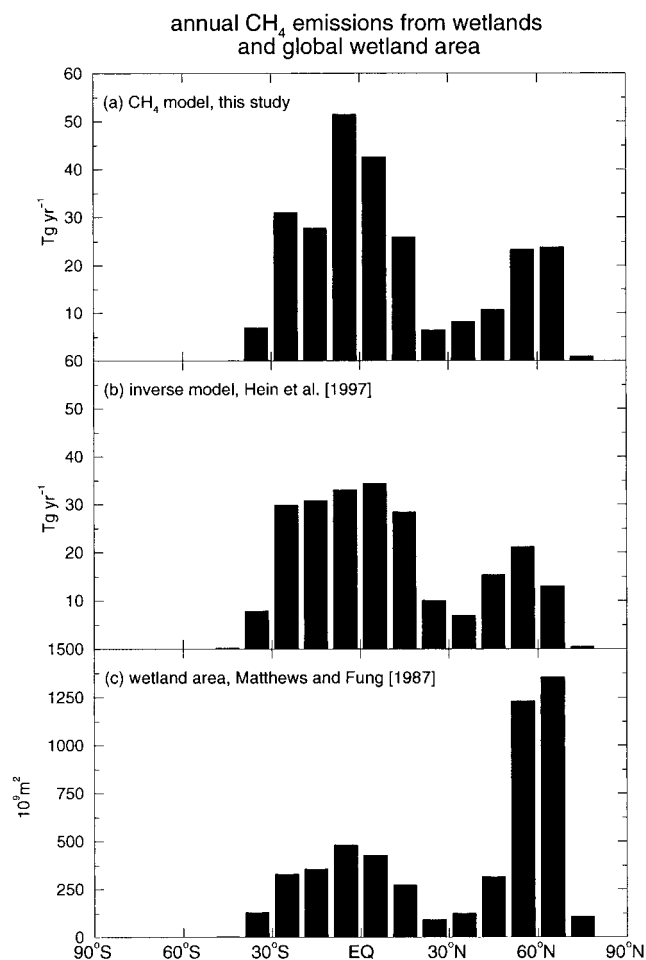


Figure 6. Zonally integrated mean annual methane emissions from wetlands (Tg yr^{-1}): (a) Modeling results from this study; (b) results from an inverse model [Hein *et al.*, 1997]; (c) zonally integrated wetland area distribution (10^9 m^2) from the data set of Matthews and Fung [1987].

(Figure 6b) shows that both methods have a peak around the equator and another peak around 60°N . A comparison with the zonally integrated wetland areas of Matthews and Fung [1987] (Figure 6c) shows that these two peaks are related to peaks in wetland areas. As discussed in section 5.2.1, Hein *et al.* [1997] give a slightly lower value for global annual methane emissions from wetlands, and the peak around the equator is less pronounced in their study than in ours. In both studies, however, about 25% of the global annual emissions originates from high northern latitude ($>30^\circ\text{N}$) wetlands (which constitute 60% of the global wetland area). Given the differences in methods between these two studies the similarity between the results suggests that they are robust.

5.2.1. Global wetland source strength. The 1983–1992 mean of simulated methane emissions is 260 Tg yr^{-1} . This value is at the high end of current estimates of the global wetland source strength. The amplitude of simulated methane emissions depends on a factor R_0 in the methane production rate; global values of R_0 are parameterized as a function of NPP and the mean annual temperature derived from six test sites where measurements of methane fluxes over at least one season were available. Compared to other studies [Bartlett and Harris, 1993; Matthews, 2000, and references therein], annual

methane emissions from these test sites seem quite high, which can explain the high global emission; a comparison with data from a Swedish mire and a Minnesota peatland presented in section 5.3 supports this hypothesis. A sensitivity test of the one-dimensional methane model, however, has shown that changes in R_0 only change the amplitude of simulated methane emissions but not the temporal emission pattern [Walter and Heimann, 2000].

“Bottom-up” approaches use flux measurements and information on emission periods and wetland areas to extrapolate to global and annual scales; estimated global methane emissions range from 80 to 156 Tg yr^{-1} [Aselmann and Crutzen, 1989; Matthews and Fung, 1987; Bartlett and Harris, 1993; Lelieveld *et al.*, 1998; Khalil and Rasmussen, 1983]. Even though seasonal and interannual variations in methane emissions are known to be high, only a few of the flux data sets used are of high frequency and cover periods of a season or more. In addition, fluxes are usually grouped on the basis of wetland and/or vegetation type; the main factors controlling methane emissions, however, are water table, temperature, and substrate quality [Conrad, 1989]. Wetland and vegetation types are certainly related to these factors; for example, vegetation affects substrate quality. However, these factors and methane fluxes can vary widely within one wetland or vegetation type. Micrometeorological measurements, for example, which cover larger spatial scales [Clement *et al.*, 1995] or a climate-sensitive model using as many measurements as possible to extrapolate to the global scale could improve “bottom-up” approaches.

In a “top-down” approach, Hein *et al.* [1997] used an inverse model to test several scenarios; they obtained a global wetland source strength of about 230 Tg yr^{-1} ($\pm 10\%$) if an a priori estimate of 270 Tg yr^{-1} was used and of 200 Tg yr^{-1} ($\pm 10\%$) if an a priori estimate of 135 Tg yr^{-1} was used; i.e., a relatively large wetland source is obtained independent of the a priori source estimate. The major limitations of inverse modeling lie in the models used, the assumptions made, and the sparse distribution of atmospheric data. As all “bottom-up” estimates agree that global wetland emissions are below 156 Tg yr^{-1} , there is an apparent discrepancy that has not yet been resolved. Another method to constrain the current wetland source strength is to use an estimate of the preindustrial wetland source. Houweling *et al.* [2000] simulated preindustrial methane employing a three-dimensional chemistry-transport model using methane mixing ratios and $\delta^{13}\text{CCH}_4$ from ice cores as constraints; they tested several scenarios of preindustrial sources and sinks and obtained a preindustrial wetland source strength of $130\text{--}194 \text{ Tg yr}^{-1}$. They point out that cultivation and drainage could have reduced the preindustrial wetland source by 10% (see references in the work of Houweling *et al.* [2000]). However, climatic changes since the beginning of industrialization could have increased global methane fluxes, as global mean temperatures have increased by about 0.7° since the late 1880s [Hansen *et al.*, 1999]. This climate-induced increase in global methane fluxes could even be larger than 10% [Walter *et al.*, this issue].

In summary, global estimates for the wetland source strength vary between 80 and 230 Tg yr^{-1} . In this study a high value of 260 Tg yr^{-1} is obtained primarily, because the six data sets used in the global extrapolation of the model show relatively high emissions. Overestimation of the global total should not compromise the capability of the model to investigate climate-induced spatial and temporal patterns, which is the purpose of this study. However, a model such as ours could be

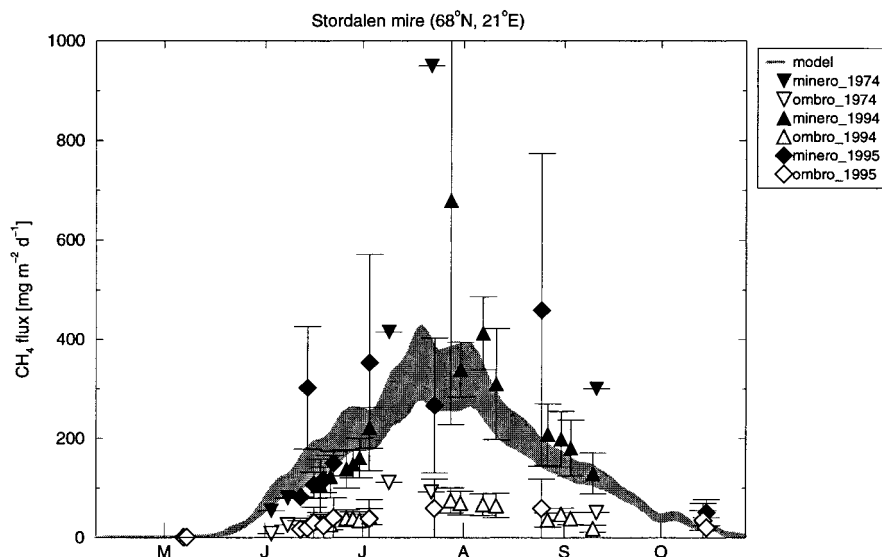


Figure 7. Test of the methane model at the Stordalen mire (Sweden) ($\text{mg m}^{-2} \text{d}^{-1}$). Comparison between the 12 year (1982–1993) average of the mean of simulated methane emissions from the Stordalen grid cell and its direct neighbors (± 1 standard deviation) (grey area) and observed methane emissions from minerotrophic (solid symbols) and ombrotrophic (open symbols) parts of the wetland for different years [Svensson *et al.*, 1999].

used to improve “bottom-up” estimates, if a different global extrapolation based on as many data as possible is used.

5.3. Model Evaluation Against Field Measurements

The one-dimensional methane model was successfully tested at six sites, where time series of the input and output data of the methane model and information on model parameters were available [Walter and Heimann, 2000]. For a test of the global methane-hydrology model, data representative of larger spatial scales are needed. Global measurements of atmospheric methane concentrations are one possibility [Walter *et al.*, this issue]. Regional estimates of annual methane emissions exist in a few places [Reeburgh *et al.*, 1998; Roulet *et al.*, 1994; Tathy *et al.*, 1992; Devol *et al.*, 1990; Bartlett *et al.*, 1988]. However, they are far too sparse, to test whether the spatial pattern of modeled methane emissions is realistic. Time series of methane emissions on spatial scales comparable to the model’s 1° by 1° grid are not available. Therefore we use two data sets consisting of time series of methane flux measurements that are representative of an entire wetland, i.e., about 1 km^2 . At both sites, chamber measurements were made in different parts of the wetland, and at one site, eddy correlation measurements were also performed.

Svensson *et al.* [1999] report methane measurements made in a subarctic Swedish mire (Stordalen mire, 68°N , 21°E) in 1974, 1994, and 1995. They measured methane fluxes in dry and wet parts and in ombrotrophic (nutrient deficient) and minerotrophic (nutrient rich) parts of the wetland. Fluxes from the dry parts were very low. In the wet parts, fluxes from minerotrophic soils were considerably larger than those from ombrotrophic soils (Figure 7). These differences are attributable to differences in soil chemistry and vegetation, since water tables and temperatures were similar at all wet sites. These measurements show how large sub-grid-scale variations can be. Modeled fluxes from the grid cell, where the wetland is located and from the immediately surrounding grid cells, were compared to

the observations. Fluxes from surrounding grid cells were included in order to prevent one particular R_0 value or another model parameter from becoming dominant. Because no modeling results are available for any of the years of observation the mean (± 1 standard deviation) of modeled methane emissions from all considered grid cells and years (1982–1993) is compared to the data (Figure 7). Since observed fluxes from all 3 years were similar, this should not compromise the comparison. Figure 7 shows that the seasonal cycle of observed methane fluxes is captured well by the model. The magnitude of the model results is comparable to the magnitude of emissions from minerotrophic soils which suggests that the six test sites used to calibrate the model, i.e., to derive R_0 were sites with high substrate quality favoring high emissions. Hence R_0 is not necessarily overestimated, but different R_0 values should be used within a grid cell to account for varying substrate quality. Global data sets to derive wetland fractions of different peat quality are still lacking. Therefore with the current model sub-grid-scale variations in model parameters such as R_0 cannot be considered. However, this needs to be improved in the future.

The data set of Clement *et al.* [1995] consists of eddy correlation and chamber measurements from a peatland in central Minnesota (Bog Lake peatland, 48°N , 93°W) made during 1991–1992. The chamber measurements were made from different hummock/hollow pair locations. The seasonal patterns of fluxes obtained by the two techniques compared well, although the magnitudes were slightly different. Upscaling of the chamber measurements using information on microtopography reduced this discrepancy. Figure 8 shows a comparison between simulated and observed methane fluxes (row 1: simulated methane emissions from the grid-cell, where the wetland is located and the surrounding grid cells are used) and water table (row 2: the observed water table is depicted relative to the average hollow surface which is about 35 cm lower than the average hummock surface); in rows 3 and 4, model input, i.e., ECMWF precipitation, and temperature are compared to

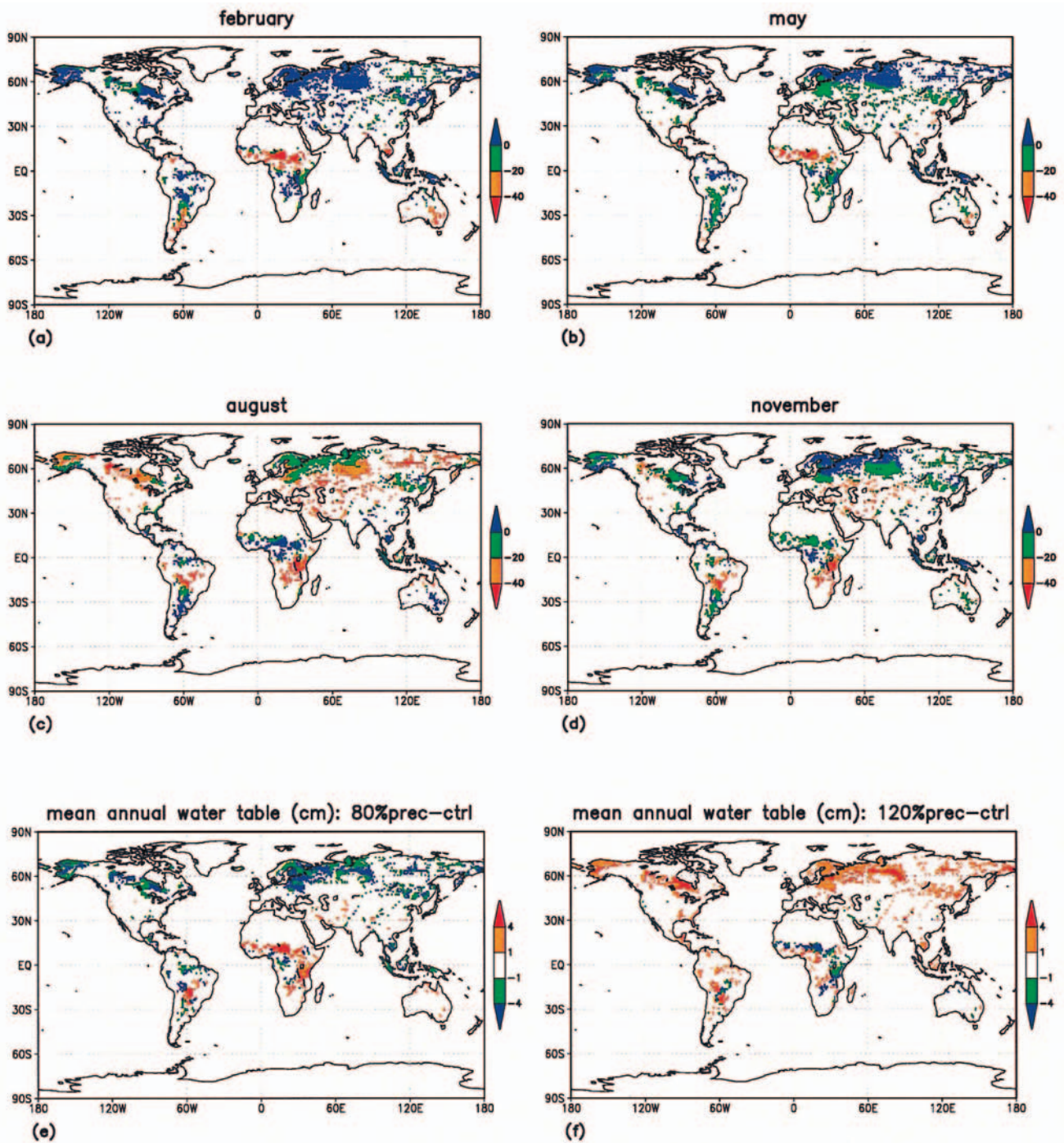


Plate 2. Seasonal variation in the water table: simulated monthly mean water table (cm) for (a) February, (b) May, (c) August, and (d) November. Sensitivity test of the hydrologic model to precipitation: Simulated annual mean water table (cm), difference between (e) 80% precipitation and control and (f) 120% precipitation and control.

observations made at the wetland site. ECMWF temperature and observed temperature are very similar. ECMWF precipitation is slightly higher than observations in 1991, but the patterns are similar. In 1992, however, ECMWF precipitation is generally lower than observations, and they differ considerably in June when observed precipitation is twice as high as ECMWF precipitation. This is an example of how large sub-grid-scale variations in precipitation can be. However, reanalysis precipitation is not always realistic [Stendel and Arpe,

1997]. These differences in the input data affect simulated water tables. In 1991 simulated and observed water table compare well. In 1992 simulated and observed water tables are similar until June when the observed water table rises to the soil surface due to extremely high precipitation in June. Because ECMWF precipitation is much lower, the simulated water table remains below the soil surface. This affects modeled methane fluxes. In 1991 the seasonal pattern of simulated and observed methane emissions agree well, the magnitude of sim-

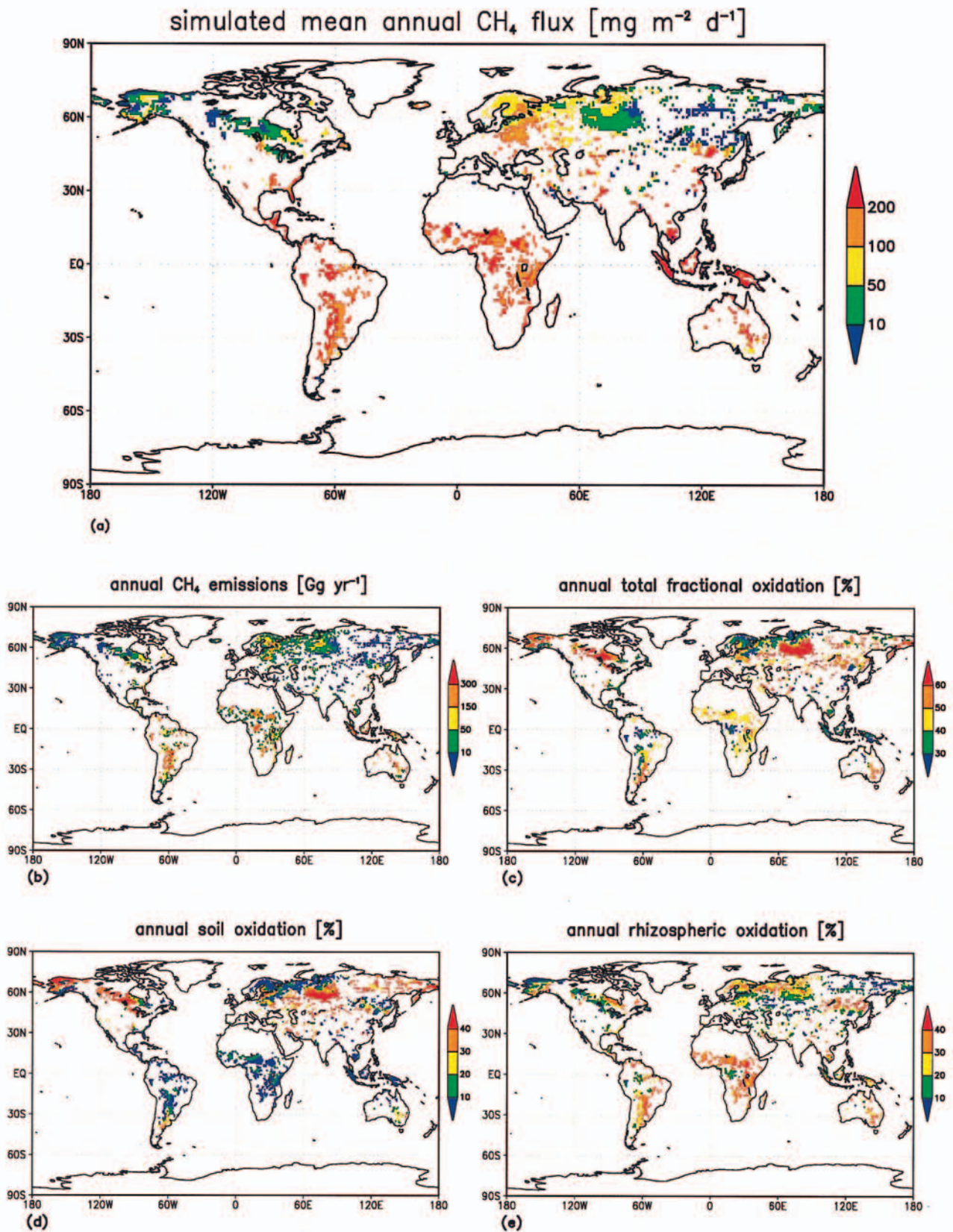


Plate 3. (a) Simulated mean annual methane fluxes ($\text{mg m}^{-2} \text{d}^{-1}$) (average of the 12 year simulation period 1982–1993). Simulated emission and oxidation of methane: (b) annual methane emissions per grid cell (Gg yr^{-1}), (c) annual total fractional oxidation (which is the sum of annual soil oxidation and annual rhizospheric oxidation) (%), (d) annual soil oxidation (%), (e) and annual rhizospheric oxidation (%).

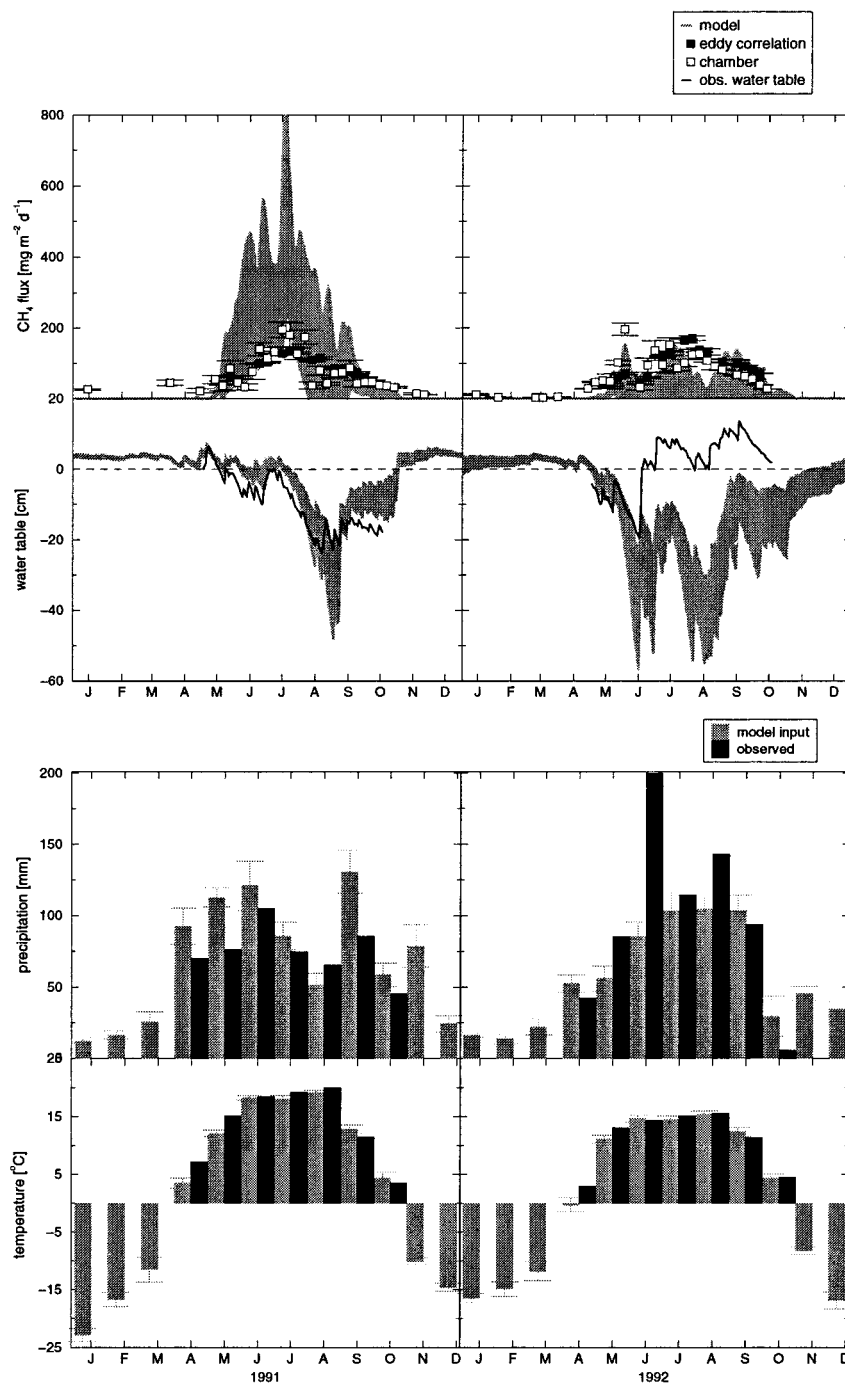


Figure 8. Test of the methane model at the Bog Lake peatland (Minnesota); all model results/model input data are the mean of the Bog Lake peatland grid cell and its direct neighbors (± 1 standard deviation) (grey areas); all observations are depicted in black. Row 1, comparison between simulated and observed methane emissions ($\text{mg m}^{-2} \text{d}^{-1}$) from chamber and micrometeorological measurements [Clement *et al.*, 1995] for 1991 and 1992; row 2, comparison between simulated water table and observed water table relative to the average hummock surface; row 3, comparison between model input monthly precipitation and observed monthly precipitation for the Bog Lake peatland; row 4, comparison between model input monthly temperature and observed monthly temperature for the Bog Lake peatland.

ulated methane emissions, however, is greater than in the observations. This implies that the R_0 values used in the model are too large and that differences in substrate quality affecting R_0 need to be included in the future. Since in 1992 the simulated water table is below the soil surface during the most productive time (June–August), simulated emissions are con-

siderably lower than in 1991. This big drop in methane emissions is not seen in the observations, because the observed water table is above the soil surface during June–August 1992. Slightly lower temperatures in 1992 also contribute to this drop in emissions, and observed methane fluxes are also slightly lower in 1992 than in 1991. However, the main difference

between observations and model results in 1992 is due to differences in the input data confirming that subgrid variations and/or limitations in the input data (mainly precipitation) can have a strong effect on modeling results.

In summary, at both test sites the seasonality of simulated and observed methane emissions agreed well. However, the results suggest that R_0 in the model is too large and that different R_0 values should be used within one grid cell to account for variations in substrate quality. In addition, subgrid-scale variations in the input data (mainly precipitation) and/or limitations in the used input data can also affect modeling results.

6. Summary and Conclusion

In this article we presented the components of a global, process-based, climate-sensitive methane-hydrology model to derive methane emissions from natural wetlands. Because the processes controlling methane production rates are not modeled explicitly, a simple method to derive spatial variations in the production rate (i.e., in R_0 of (1)) from annual NPP and soil temperature was developed. In the future a model to derive R_0 from biogeochemical, biogeographical, and climatic variables could be used to replace (2). However, to do so, more needs to be known about quantitative relationships between these parameters and R_0 , and data on the global distribution of factors affecting R_0 need to become available.

The model was applied to the global wetland distribution of Matthews and Fung [1987]. Global data sets of all model parameters (efficiency of plant-mediated transport, rooting depth, soil depth, and relative pore space) were developed from existing global data sets of vegetation [Wilson and Henderson-Sellers, 1985] and soil characteristics [Dunne and Wilmott, 1996]. Efficiency of plant-mediated transport was derived from the still sparse knowledge about the gas-conducting properties of different plants. Rooting depth and soil depth were determined from vegetation-related vertical distributions of root biomass. Relative pore space was derived from a global data set on soil texture. All these parameters are not homogeneously distributed within a 1° by 1° grid cell and few data sets consider the special conditions prevailing in wetlands. Hence higher-resolution data sets might help to improve global data sets of the model parameters in the future.

A simple hydrologic model to derive the variation of the water table in wetlands was developed. The model is based on assumptions made for wetland conditions. No data set comprising input and output data of the model has been available. Therefore simulated variations in the water table of a grid cell were compared to point measurements obtained within the same grid cell. Nonetheless, in the limitations of this comparison, it could be shown that the hydrologic model calculates realistic seasonal cycles in the water table. Different variations of the water yield coefficient ($C_{wy}(z)$ in (9)) should be tested in the future. A sensitivity test of the hydrologic model showed that the effect of a $\pm 20\%$ change in precipitation varies between different sites. In general, greater precipitation leads to higher water levels, and vice versa, and the effect of a $\pm 20\%$ change in precipitation is higher in the HNH wetlands. However, in regions where the difference between total annual precipitation and total annual potential evapotranspiration (PmE) is negative, the opposite can be the case. In these regions, lateral inflow (L in (17)), which is inversely related to precipitation, is different from zero. Hence lower precipitation

can lead to a higher water table, which occurs in some African and South American wetlands. Since this effect occurs mainly during the dry season, it is not expected to have a large impact on modeled methane emissions. However, it will be fixed in future versions of the hydrologic model. Simulated water levels in HNH wetlands are highest during the winter and lowest during the summer. In the tropics, there is usually standing water during the wet season and very low (often below 1 m soil depth) water levels during the dry season. The amplitude of seasonal variations in the water table is, in general, larger in tropical wetlands. Because of microtopography the position of the water table relative to the soil surface is not constant throughout a wetland. This effect has not yet been considered in the hydrologic model and should be included in future versions.

The model has been applied using the ECMWF reanalyses of the period 1982–1993 as climate forcing. We calculated total annual methane emissions from wetlands to be 260 Tg yr^{-1} , which is larger than other estimates. Annual methane fluxes are lower in higher latitudes because of the shorter productive period, and HNH emissions constitute about 25% of the total wetland emissions. On a global and annual basis, only 60% of the produced methane is emitted, the rest is reoxidized in soil. A comparison between the meridional pattern of calculated annual methane emissions with a result from an inverse modeling study [Hein *et al.*, 1997] shows good agreement.

Our modeling results are compared to data from two wetlands in Sweden and Minnesota. At both test sites the seasonality of simulated and observed methane emissions agreed well. However, these tests demonstrate the effect of subgrid variations in model parameters and input data on methane emissions. The results suggest that the parameter R_0 in the model is too large and that a suite of R_0 values should be used within grid cells to account for variations in substrate quality. In addition, subgrid variations in the input data (mainly precipitation) and/or limitations in the input data can also affect modeling results. Higher-resolution data sets are needed to improve this in the future.

Acknowledgments. B. Walter wishes to thank P. Frenzel for his assistance in creating the global data set on plant-mediated transport. Thanks also to A. Kleidon and W. Knorr for useful discussions, to M. Stendel and U. Schulzweida for help with the ECMWF reanalysis data, and to M. Letts for informative discussions about the hydrologic model. Additionally, the authors wish to thank N. Roulet and the other reviewers for their comments, which were particularly helpful in improving this manuscript. The used ECMWF reanalyses were provided by the European Centre for Medium-Range Weather Forecasts in cooperation with the Deutsche Wetter Dienst (DWD). This work was supported by the German Bundesministerium für Bildung, Wissenschaft, Forschung und Technologie (BMBF) as part of the Klimaschutzprogramm “Spurenstoffkreisläufe” and by the NASA Atmospheric Chemistry, Modeling and Analysis Program (ACMAP).

References

- Aselmann, I., and P. J. Crutzen, Global distribution of natural freshwater wetlands and rice paddies, their Net Primary Productivity, seasonality and possible methane emissions, *J. Atmos. Chem.*, 8, 307–358, 1989.
- Bartlett, K. B., and R. C. Harriss, Review and assessment of methane emissions from wetlands, *Chemosphere*, 26, 1–4, 261–320, 1993.
- Bartlett, K. B., P. M. Crill, D. I. Sebacher, R. C. Harriss, J. O. Wilson, and J. M. Melack, Methane flux from the central Amazonian floodplain, *J. Geophys. Res.*, 93, 1571–1582, 1988.
- Boelter, D. H., Important physical properties of peat materials, in *Proceedings of the Third International Peat Congress*, Dep. of Energy,

- Mines and Resour. Canada, Natl. Res. Counc. of Canada, Ottawa, 1968.
- Bogner, J. E., R. L. Sass, and B. P. Walter, Model comparisons of methane oxidation across a management gradient: Wetlands, rice production systems, and landfills, *Global Biogeochem. Cycles*, *14*(4), 1021–1033, 2000.
- Cao, M., S. Marshall, and K. Gregson, Global carbon exchange and methane emission from natural wetlands: Application of a process-based model, *J. Geophys. Res.*, *101*, 14,399–14,414, 1996.
- Clement, R. J., S. B. Verma, and E. S. Verry, Relating chamber measurements to eddy correlation measurements of methane flux, *J. Geophys. Res.*, *100*, 21,047–21,056, 1995.
- Conrad, R., Control of methane production in terrestrial ecosystems, in *Exchange of Trace Gases Between Terrestrial Ecosystems and the Atmosphere*, edited by M. O. Andreae and D. S. Schimel, pp. 39–58, John Wiley, New York, 1989.
- Devol, A. H., J. E. Richey, B. R. Forsberg, and L. A. Martinelli, Seasonal dynamics of methane emissions from the Amazon River floodplain to the troposphere, *J. Geophys. Res.*, *95*, 16,417–16,426, 1990.
- Dise, N. B., Methane emission from Minnesota peatlands: Spatial and seasonal variability, *Global Biogeochem. Cycles*, *7*(1), 123–142, 1993.
- Dlugokencky, E. J., K. A. Masarie, P. M. Lang, and P. P. Tans, Continuing decline in the growth rate of atmospheric methane, *Nature*, *393*, 447–450, 1998.
- Dunne, K. A., and C. J. Willmott, Global distribution of plant-extractable water capacity of soil, *Int. J. Climatol.*, *16*, 16,841–16,859, 1996.
- Edwards, M. O., Global gridded elevation and bathymetry (ETOPO5), Digital raster data on a 5-minute geographic (lat/lon) 2160*4320 (centroid-registered) grid, NOAA Natl. Geophys. Data Cent., Boulder, Colo., 1989.
- Food and Agriculture Organization (FAO)/UNESCO, *1971–1981: Soil Map of the World*, vols. 1–10, Paris, France, 1971–1981.
- Federer, C. A., Transpirational supply and demand: Plant, soil, and atmospheric effects evaluated by simulation, *Water Resour. Res.*, *18*, 355–362, 1982.
- Gale, M. R., and D. F. Grigal, Vertical root distributions of northern tree species in relation to successional status, *Can. J. Forest Res.*, *17*, 829–834, 1987.
- Gibson, J. K., P. Källberg, S. Uppala, A. Hernandez, A. Nomura, and E. Serrano, The ECMWF Re-Analysis (ERA), 1, ERA description, *ECMWF Re-Anal. Proj. Rep. Ser.*, *1*, 71 pp., Eur. Cent. for Medium-Range Weather Forecasts, Reading, England, 1997.
- Hansen, J., R. Ruedy, J. Glasco, and M. Sato, GISS analysis of surface temperature change, *J. Geophys. Res.*, *104*, 30,997–31,022, 1999.
- Hartge, K. H., and R. Horn, *Einführung in die Bodenphysik*, Ferdinand Enke, Stuttgart, Germany, 1991.
- Hein, R., P. J. Crutzen, and M. Heimann, An inverse modeling approach to investigate the global atmospheric methane cycle, *Global Biogeochem. Cycles*, *11*(1), 43–76, 1997.
- Hogan, K., and R. Harriss, Comment on “A dramatic increase in the growth rate of atmospheric methane in the northern hemisphere during 1992,” by E. J. Dlugokencky et al., *Geophys. Res. Lett.*, *21*, 2445–2446, 1994.
- Houweling, S., F. Dentener, and J. Lelieveld, Simulation of preindustrial atmospheric methane to constrain the global source strength of natural wetlands, *J. Geophys. Res.*, *105*, 17,243–17,255, 2000.
- Jackson, R. B., J. Canadell, J. R. Ehleringer, H. A. Mooney, O. E. Sala, and E. D. Schulze, A global analysis of root distributions for terrestrial biomes, *Oecologia*, *108*(3), 389–411, 1996.
- Jouzel, J., et al., Extending the Vostock ice-core record of paleoclimate to the penultimate glacial period, *Nature*, *364*, 407–412, 1993.
- Kaduk, J., Simulation der Kohlenstoffdynamik der globalen Landbiosphäre mit SILVAN-Modellbeschreibung und Ergebnisse, dissertation, Max-Planck-Inst. für Meteorol., Hamburg, Germany, 1996.
- Khalil, M. A. K., and R. A. Rasmussen, Sources, sinks and seasonal cycles of atmospheric methane, *J. Geophys. Res.*, *88*, 5131–5144, 1983.
- Knorr, W., Satellite remote sensing and modelling of the global CO₂ exchange of land vegetation: A synthesis study, dissertation, Max-Planck-Inst. für Meteorol., Hamburg, Germany, 1997.
- Lelieveld, J., P. J. Crutzen, and F. J. Dentener, Changing concentration, lifetime and climate forcing of atmospheric methane, *Tellus, Ser. B*, *50*, 128–150, 1998.
- Letts, M. G., N. T. Roulet, N. T. Comer, M. R. Skarupa, and D. L. Verseghy, Parametrization of peatland hydraulic properties for the Canadian Land Surface Scheme, *Atmos. Ocean*, *38*(1), 141–160, 2000.
- Matthews, E., Wetlands, in *Atmospheric Methane: Its Role in the Global Environment*, edited by M. A. K. Khalil, pp. 202–233, Springer-Verlag, New York, 2000.
- Matthews, E., and I. Fung, Methane emission from natural wetlands: Global distribution, area, and environmental characteristics of sources, *Global Biogeochem. Cycles*, *1*(1), 61–86, 1987.
- Mitsch, W. J., and J. G. Gosselink, *Wetlands*, Van Nostrand Reinhold, New York, 1993.
- Murray, F. W., On the computation of saturation vapour pressure, *J. Appl. Meteorol.*, *6*, 203–204, 1967.
- Ramachandran, P., and R. Ramachandran, Methane emission inventory from tropical coastal wetlands (Mangrove ecosystems), poster presented at the Joint International Symposium on Global Atmospheric Chemistry, CACGP and IGAC, Seattle, Wash., 1998.
- Reeburgh, W. S., J. Y. King, S. K. Regli, G. W. King, N. A. Auerbach, and D. A. Walker, A CH₄ emission estimate for the Kuparuk River basin, Alaska, *J. Geophys. Res.*, *103*, 29,005–29,013, 1998.
- Roulet, N. T., A. Jano, C. A. Kelly, L. F. Klinger, T. R. Moore, R. Protz, J. A. Ritter, and W. R. Rouse, Role of the Hudson Bay lowland as a source of atmospheric methane, *J. Geophys. Res.*, *99*, 1439–1454, 1994.
- Saarnio, S., J. Alm, J. Silvola, A. Lohila, H. Nykänen, and P. J. Martikainen, Seasonal variation in CH₄ emissions and production and oxidation potentials at microsites of an oligotrophic pine fen, *Oecologia*, *110*, 414–422, 1997.
- Schimel, J. P., Plant transport and methane production as controls on methane flux from arctic wet meadow tundra, *Biogeochemistry*, *28*, 183–200, 1995.
- Schütz, H., W. Seiler, and R. Conrad, Processes involved in formation and emission of methane in rice paddies, *Biogeochemistry*, *27*, 35–60, 1989.
- Severinghaus, J. P., and E. J. Brook, Abrupt climate change at the end of the last glacial period inferred from trapped air in polar ice, *Science*, *286*(5441), 930–934, 1999.
- Severinghaus, J. P., T. Sowers, E. J. Brook, R. B. Alley, and M. L. Bender, Timing of abrupt climate change at the end of the Younger Dryas interval from thermally fractionated gases in polar ice, *Nature*, *391*, 141–146, 1998.
- Shannon, R. D., and J. R. White, A three-year study of controls on methane emissions from two Michigan peatlands, *Biogeochemistry*, *27*, 35–60, 1994.
- Shannon, R. D., J. R. White, J. E. Lawson, and B. S. Gilmour, Methane efflux from emergent vegetation in peatlands, *J. Ecol.*, *84*(2), 239–246, 1996.
- Slatyer, R. O., and I. C. McIlroy, *Practical Micrometeorology*, UNESCO, Paris, France, 1961.
- Stendel, M., and K. Arpe, Evaluation of the hydrological cycle in reanalyses and observations, *Rep. 228*, 52 pp., Max-Planck-Inst. für Meteorol., Hamburg, Germany, 1997.
- Svensson, B. H., T. R. Christensen, E. Johansson, and M. Öquist, Interdecadal variations in CO₂ and CH₄ exchange of a subarctic mire—Stordalen revisited after 20 years, *Oikos*, *85*, 22–30, 1999.
- Tathy, J.-P., B. Cros, R. A. Delmas, A. Marenco, J. Servant, and M. Labat, Methane emission from flooded forest in Central Africa, *J. Geophys. Res.*, *97*, 6159–6168, 1992.
- Valentine, D. W., E. A. Holland, and D. S. Schimel, Ecosystem and physiological controls over methane production in northern wetlands, *J. Geophys. Res.*, *99*, 1563–1571, 1994.
- Veihmeyer, F. J., and A. H. Hendrickson, The moisture equivalent as a measure of the field capacity of soils, *Soil Sci.*, *32*, 181–193, 1931.
- Walter, B. P., M. Heimann, R. D. Shannon, and J. R. White, A process-based model to derive methane emissions from natural wetlands, *Geophys. Res. Lett.*, *23*(25), 3731–3734, 1996.
- Walter, B. P., Development of a process-based model to derive methane emissions from natural wetlands for climate studies, dissertation, Max-Planck-Inst. für Meteorol., Hamburg, Germany, 1998.
- Walter, B. P., and M. Heimann, A process-based, climate-sensitive model to derive methane emissions from natural wetlands: Application to five wetland sites, sensitivity to model parameters, and climate, *Global Biogeochem. Cycles*, *14*(3), 745–765, 2000.
- Walter, B. P., M. Heimann, and E. Matthews, Modeling modern meth-

- ane emissions from natural wetlands, 2, Interannual variations 1982–1993, *J. Geophys. Res.*, this issue.
- Whalen, S. C., and W. S. Reeburgh, Interannual variations in tundra methane emissions: A four-year time series at fixed sites, *Global Biogeochem. Cycles*, 6, 139–159, 1992.
- Wilson, M. F., and A. Henderson-Sellers, A global archive of land cover and soils data for use in general circulation models, *J. Climatol.*, 5, 119–143, 1985.
- Zobler, L., A world soil file for global climate modeling, Tech. Mem. 87802, NASA, 1986.
-
- E. Matthews and B. P. Walter, NASA Goddard Institute for Space Studies, 2880 Broadway, New York, NY 10025. (bwalter@giss.nasa.gov)
- M. Heimann, Max-Planck-Institut für Biogeochemie, Jena, Germany.

(Received August 14, 2000; revised February 20, 2001; accepted February 22, 2001.)